HTD-Vol. 207, Fundamental Problems in Conduction Heat Transfer
ASME 1992

# THERMAL CONSTRICTION RESISTANCE OF ISOTHERMAL CIRCULAR DISKS WITH INSULATED BACK FACE AND EXTENSIONS

**M. M. Yovanovich and Peter Teertstra**
Department of Mechanical Engineering
University of Waterloo
Waterloo, Ontario, Canada

## ABSTRACT

A numerical solution employing oblate spheroidal coordinates for the Laplace equation in the region surrounding an isothermal circular disk is presented. Mixed boundary conditions on the lower disk surface represent a radially varying insulation layer which moves the solution between its full space and half space limits. The finite volume method used for the analysis is compact and displays excellent convergence characteristics for all cases considered. Using the results of the numerical work, dimensionless constriction resistance is calculated as a function of a non-dimensional insulation radius between the limits 0 and $\infty$. Correlation equations are formulated which explicitly predict dimensionless constriction resistance for the full range of insulation cases considered. Numerical solution accuracy is very good, as verified at three limiting cases with differences between the constriction resistance calculated and the exact values not exceeding 0.7%.

## NOMENCLATURE

| | | |
|---|---|---|
| $a$ | = | disk radius |
| $a_i$ | = | insulation radius |
| $A_i$ | = | surface area of insulation |
| $A_w$ | = | wetted surface area (active heat transfer area) |
| $C_i$ | = | finite volume diffusion coefficients ($i = 1-4, S$) |
| $D$ | = | finite volume source coefficient |
| $i$ | = | nodal point index in $\eta$ direction |
| $j$ | = | nodal point index in $\theta$ direction |
| $k$ | = | thermal conductivity |
| $Nu$ | = | Nusselt number |
| $P$ | = | heat generation per unit volume |
| $q$ | = | heat flux |
| $Q$ | = | total heat flow rate |
| $r$ | = | radial coordinate |
| $R$ | = | thermal constriction resistance |
| $R^*$ | = | dimensionless constriction resistance ($Rka$) |
| $S$ | = | shape factor |
| $S^*$ | = | dimensionless shape factor |
| $T$ | = | temperature (numerical model) |
| $V$ | = | volume |
| $z$ | = | axial coordinate |
| $\epsilon$ | = | ratio of insulation radius to disk radius ($a_i/a$) |
| $\eta$ | = | oblate spheroidal coordinate |
| $\theta$ | = | oblate spheroidal coordinate |
| $\Delta\eta$ | = | nodal increment, $\eta$ direction |
| $\Delta\theta$ | = | nodal increment, $\theta$ direction |
| $\phi$ | = | dimensionless temperature $(T - T_\infty)/(T_0 - T_\infty)$ |
| $\zeta$ | = | correlation coefficient |
| $\xi$ | = | correlation coefficient |
| $\delta_r$ | = | solution residual (numerical model) |

*Subscripts*

| | | |
|---|---|---|
| $i, j$ | = | at the nodal location indexed by $(i, j)$ |
| 0 | = | at the body surface |
| $\infty$ | = | at points far from the body |

## INTRODUCTION

Steady-state conduction from an isothermal circular disk of radius $a$ which has one face partially or fully insulated into an isotropic conducting medium of thermal conductivity $k$ is currently of some interest to thermal analysts who are concerned with developing models of natural convection heat transfer from a single horizontal disk. As the Rayleigh number decreases and approaches very small values ($Ra < 1$) the Nusselt number approaches the diffusive asymptote which corresponds to pure conduction from the active face of the disk into the surrounding full space. This problem is encountered in microelectronics and in the development of micron-sized temperature, pressure and flow sensors where the characteristic length of the sensor is of order 10 *microns* or less. Solutions for both the partially insulated case and the fully insulated case with side extensions are not available presently.

## PROBLEM SOLUTION

### Problem Statements

The problems of interest here, as displayed in Figure 1, can be formulated in circular cylinder coordinates $(r, z)$. The dimensionless temperature $\phi(r,z) = (T(r,z) - T_\infty)/(T_0 - T_\infty)$, where $T_0$ and $T_\infty$ are the disk and reference temperatures respectively, is the solution of the Laplace equation:

$$\frac{\partial^2\phi}{\partial r^2} + \frac{1}{r}\frac{\partial\phi}{\partial r} + \frac{\partial^2\phi}{\partial z^2} = 0 \qquad (1)$$

within the limits:

$$0 \le r < \infty, \qquad -\infty < z < \infty$$

The solutions $\phi(r, z^+), \phi(r, z^-)$ must satisfy the symmetry boundary condition along the axis:

$$r = 0, \qquad -\infty < z < \infty, \qquad \frac{\partial\phi}{\partial r} = 0$$

as well as the regular condition $\phi(r,z) \to 0$ as $\sqrt{r^2+z^2} \to \infty$.

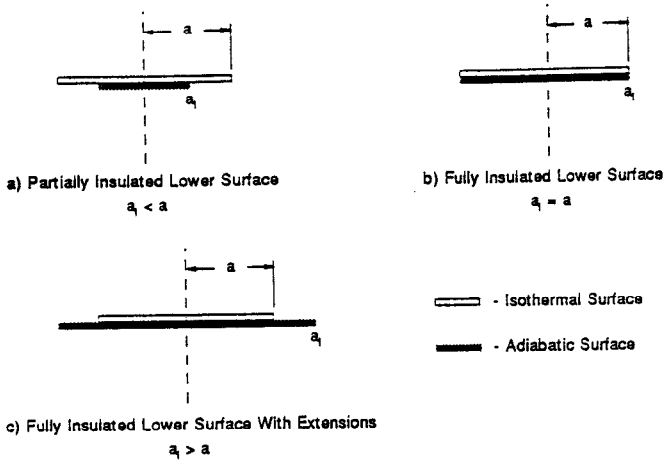


Fig. 1 Schematics of Physical Problems

Partially Insulated Disk. For the case of the isothermal disk with a partially insulated back surface (Figure 1a), a Dirichlet condition must be applied on the positive side (upper surface) of the disk:

$$z = 0, \qquad 0 \le r \le a, \qquad \phi = 1$$

On the negative side (lower surface) of the disk mixed boundary conditions (Neumann and Dirichlet) must be satisfied together:

$$z = 0, \qquad 0 \le r \le a_i \le a, \qquad \frac{\partial\phi}{\partial z} = 0$$

$$a_i < r \le a, \qquad \phi = 1$$

where $a_i$ is the insulation radius.

Fully Insulated Back Face With Side Extensions. The second problem considers a disk with a fully-insulated back face from which the insulation extends beyond the disk radius $(a_i \ge a)$, as in Figure 1c. On the upper surface of the disk and insulation mixed boundary conditions must now be satisfied:

$$z = 0, \qquad 0 \le r \le a, \qquad \phi = 1$$

$$a \le r \le a_i, \qquad \frac{\partial\phi}{\partial z} = 0$$

On the lower surface of the disk a homogeneous Neumann condition is applied:

$$z = 0, \qquad 0 \le r \le a_i, \qquad \frac{\partial\phi}{\partial z} = 0$$

It is expected that for $(a_i/a) > 6$ the solution will approach the classical isothermal solution of a circular disk on a half-space.

Constriction Resistance, Shape Factor, Diffusive Limit. A parameter of interest in this study is the thermal constriction resistance defined as:

$$R = \frac{(T_0 - T_\infty)}{Q} \qquad (2)$$

where $Q$ is the total heat transfer rate through the active heat transfer area $A_w$:

$$Q = \iint_{A_w} -k(T_0 - T_\infty)\frac{\partial\phi}{\partial z}\,dA \qquad (3)$$

The dimensionless constriction resistance is defined as:

$$R^* = Rka = \frac{a}{\iint_{A_w} -\frac{\partial\phi}{\partial z}\,dA} \qquad (4)$$

with respect to the disk radius $a$. The inverse of the dimensionless constriction resistance gives us the dimensionless shape factor:

$$S^* = \frac{S}{a} \qquad (5)$$

which comes from the definition:

$$Q = Sk(T_0 - T_\infty) \qquad (6)$$

and the diffusive Nusselt number which is defined as:

$$Nu = \frac{Qa}{A_w k(T_0 - T_\infty)} \qquad (7)$$

It is apparent from the definitions that $S^* = Nu = 1/R^*$.

### Numerical Solution

Since the analytic solution to the isothermal disk in a full space with varying insulation on its back surface is not currently available, a numeric solution is sought. The method of finite volumes is used to develop a solution to the temperature field in the region surrounding the disk, allowing thermal constriction resistance to be calculated.

Coordinate Selection for Numerical Solution. In considering heat conduction for an arbitrary geometry, the correct choice of coordinate system can greatly simplify the analytic solution to the problem. In the case of the circular disk in a

full space, the use of oblate spheroidal coordinates in the numeric solution is vital in order to ensure accurate results with the computing resources available. By using the coordinate transformations:

$$r = a\cosh\eta\sin\theta$$
$$z = a\sinh\eta\cos\theta$$

for the uninsulated isothermal disk problem it can be shown that the solution becomes one-dimensional. Although this degree of simplification is not anticipated for the more complex model corresponding to a disk which is partially insulated, certain benefits arise when this coordinate system is employed for the numeric solution. From the analytic solution to the heat flux distribution at the surface of an isothermal circular disk it can be shown that near the edge of the disk substantial variations in the magnitude of the flux occur. By using a simple grid of uniformly spaced control volumes, the oblate spheroidal coordinate system automatically introduces additional discretization in the regions of interest, adjacent to the disk in the $\eta$ direction and near the edge of the disk in the $\theta$ direction, without adding an unnecessarily fine grid in any other part of the solution domain. As well, by using this coordinate system, the disk is reduced to a planar (infinitely thin) body as required by the analytic solution in the full space.

On a qualitative basis it can be said that a solution to the circular disk problem which incorporates the oblate spheroidal coordinate system is from a physical standpoint better able to predict heat flux and temperature fields in the region surrounding the disk. As can be seen from Figure 2 , the mesh of orthogonal elliptic and hyperbolic curves should correspond in some general sense to the isotherms and flux lines in the solution region; that is, this coordinate system should be inherently better able to predict the heat flow from a circular disk to a full space than either polar or cartesian coordinates.

Finite Volume Formulation. The finite volume equations used in this solution are formulated using energy conservation principles on finite control volumes within the solution domain. The discretization chosen in this analysis divides the region in the $\eta$ and $\theta$ directions by constant intervals $\Delta\eta$ and $\Delta\theta$ to create a mesh of uniform control volumes, as shown in Figure 2. Nodal locations are spatially characterized by the notation $(i,j)$, where $i$ and $j$ indicate discrete locations in the $\eta$ and $\theta$ directions respectively. Interior control volumes are labelled starting at $i = 2$ and $j = 2$, with the index $i = 1$ and $j = 1$ being reserved for boundary control volumes.

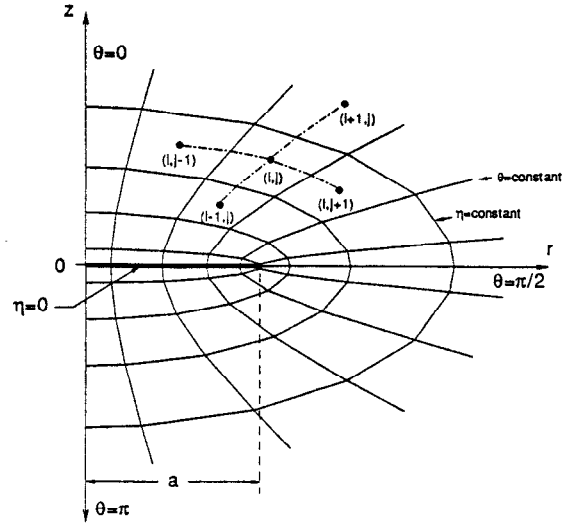

Fig. 2 Finite Volume Mesh in Oblate Spheroidal Coordinates

For the axi-symmetric, steady state model considered in this analysis, the first law of thermodynamics for an arbitrary control volume can be written as:

$$Q_{i-\frac{1}{2},j} - Q_{i+\frac{1}{2},j} + Q_{i,j-\frac{1}{2}} - Q_{i,j+\frac{1}{2}} + \iiint_{CV} P\,dV = 0 \quad (8)$$

where $Q_{i-\frac{1}{2},j}$, for example, represents the total heat flow in the positive $i$ direction across the control surface located along the $\eta$ coordinate corresponding to the discretized location $i-\frac{1}{2}$ and P represents a source or generation term integrated over the control volume.

Using first order approximations between nodes for the temperature derivatives which occur within the heat flow terms, an algebraic equation is established linking the central node temperature to that of its four surrounding neighbors (the formulation of the finite volume equations in general orthogonal curvilinear coordinates is presented in detail in reference (1) ). Then, the energy balance can be written as:

$$C_1T_{i-1,j} + C_2T_{i+1,j} + C_3T_{i,j-1} + C_4T_{i,j+1} + C_ST_{i,j} + D = 0 \quad (9)$$

In oblate spheroidal coordinates using a fully implicit formulation, the coefficients are determined for interior, non-boundary control volumes:

$$C_1 = \frac{\cosh(\eta_{i-\frac{1}{2},j})}{(\Delta\eta)_{i-1,j}}\left(\cos(\theta_{i,j-\frac{1}{2}}) - \cos(\theta_{i,j+\frac{1}{2}})\right)$$
$$C_2 = \frac{\cosh(\eta_{i+\frac{1}{2},j})}{(\Delta\eta)_{i+1,j}}\left(\cos(\theta_{i,j-\frac{1}{2}}) - \cos(\theta_{i,j+\frac{1}{2}})\right)$$
$$C_3 = \frac{\sin(\theta_{i,j-\frac{1}{2}})}{(\Delta\theta)_{i,j-1}}\left(\sinh(\eta_{i+\frac{1}{2},j}) - \sinh(\eta_{i-\frac{1}{2},j})\right)$$
$$C_4 = \frac{\sin(\theta_{i,j+\frac{1}{2}})}{(\Delta\theta)_{i,j+1}}\left(\sinh(\eta_{i+\frac{1}{2},j}) - \sinh(\eta_{i-\frac{1}{2},j})\right)$$
$$C_S = -\sum_{n=1}^{4} C_n$$
$$D = 0$$

The following examples describe the notation used in this formulation. The expression $\eta_{i+\frac{1}{2},j}$ represents the eta-coordinate of the control volume boundary facing the neighboring $i+1,j$ control volume. $\theta_{i,j-\frac{1}{2}}$ denotes the control surface adjacent to the $i,j-1$ control volume, and $(\Delta\eta)_{i-1,j}$ and $(\Delta\theta)_{i,j+1}$ represent node-to-node distances between the central control volume and its neighbors in the negative $i$ and positive $j$ directions respectively. Since no sources are included for any interior control volumes, the coefficient $D$ is set to zero in the initial development.

The control volume equation developed above is valid for all interior control volumes except those with control surfaces which contact the physical boundaries of the solution domain. For these special cases the effects of the thermal boundary conditions must be added to the energy balance in order to

close the equation set.

Boundary Conditions. The boundary conditions as established by both the the physical boundaries of the problem and the axi-symmetric nature of the model are applied using energy conservation techniques at the boundary regions. For each interior control volume that contacts a boundary an additional control surface and nodal point are added to the model at a position corresponding to the intersection of the interior control volume and the boundary. For these special boundary control volumes, an energy balance can be performed as in the previous section to yield the following expression for the example of a boundary control volume adjacent to the disk ($\eta = 0$) indexed as ($i = 1, j$):

$$C_2^{i=1,j} T_{2,j} + C_S^{i=1,j} T_{1,j} + D^{i=1,j} = 0 \qquad (10)$$

This formulation relates the temperature at the first interior control volume, denoted $2, j$, with the temperature and source term associated with the boundary node indexed as $1, j$. Superscript labels on the energy balance coefficients follow the same index convention.

In order to apply the boundary energy balance into the solution domain of interior control volumes for this example, it is substituted into the control volume energy balance ( Equation 9), yielding the following:

$$C_1^{i=2,j}\left[-\frac{C_2^{i=1,j}}{C_S^{i=1,j}} T_{2,j} - \frac{D^{i=1,j}}{C_S^{i=1,j}}\right] + C_2^{i=2,j} T_{3,j} + C_3^{i=2,j} T_{2,j-1} + C_4^{i=2,j} T_{2,j+1} + C_S^{i=2,j} T_{2,j} + D^{i=2,j} = 0 \qquad (11)$$

$$\left[C_S^{i=2,j} - C_1^{i=2,j}\frac{C_2^{i=1,j}}{C_S^{i=1,j}}\right] T_{2,j} + C_2^{i=2,j} T_{3,j} + C_3^{i=2,j} T_{2,j-1} + C_4^{i=2,j} T_{2,j+1} + \left[D^{i=2,j} - C_1^{i=2,j}\frac{D^{i=1,j}}{C_S^{i=1,j}}\right] = 0 \qquad (12)$$

As can be seen above, when this substitution is complete, dependence on the boundary node temperature is eliminated.

The following descriptions present the physical nature of each of the boundary conditions used in the model, the index of the control volumes affected, and the coefficients of energy balance equation at the boundary control volume. Using the coefficients indicated, the boundary condition elimination can be performed as described previously in order to close the equation set.

i. Due to the model symmetry about the vertical axis, the surfaces defined by $\theta = 0$ and $\pi$ will be treated as zero flux (adiabatic) boundaries. For an energy balance performed on a control volume coincident with the boundary $\theta = 0$ (interior control volume indexed $(i, j = 2)$) an adiabatic boundary condition is specified by:

$$C_4^{i,j=1} = \left(-C_S^{i,j=1}\right) = 1, \qquad D^{i,j=1} = 0$$

For control volumes adjacent to the $\theta = \pi$ boundary, indexed as $(i, J)$, zero flux is applied by setting:

$$C_3^{i,J+1} = \left(-C_S^{i,J+1}\right) = 1, \qquad D^{i,J+1} = 0$$

where $J$ is the label of the last interior control volume in the $j$ direction in the interior domain.

ii. In order to model an infinite depth of field for the steady state problem, a prescribed zero temperature boundary was required for $\sqrt{r^2 + z^2} \to \infty$. From previous work(2) it was determined that sufficient field depth is attained for the steady state solution by assuming $\eta = 8$ and setting the prescribed temperature boundary at this point. It should be noted that in terms of radial dimensions, this field depth corresponds to approximately 1500 times the radius of the disk. For the prescribed zero temperature boundary along the interior control volumes $(I, j)$, the coefficients of the energy balance are set as:

$$C_1^{I+1,j} = 0, \qquad \left(-C_S^{I+1,j}\right) = 1, \qquad D^{I+1,j} = \phi_\infty = 0$$

When the boundary condition elimination is performed for the $(I, j)$ control volumes, the effects of the Dirichlet boundary are transferred to the source coefficient $D^{I,j}$.

iii. The prescribed isothermal temperature boundary condition applied at $\eta = 0$ is treated in a manner similar to the $\sqrt{r^2 + z^2} \to \infty$ boundary. The energy balance is is satisfied for the Dirichlet condition by setting the coefficients as:

$$C_1^{i=1,j} = 0, \qquad \left(-C_S^{i=1,j}\right) = 1, \qquad D^{i=1,j} = \phi_0 = 1,$$

where the interior control volumes affected by the boundary condition elimination are indexed $(i = 2, j)$.

iv. Mixed boundary conditions will occur on the lower surface of the disk at $\eta = 0$ for the case $0 < a_i < a$. The Dirichlet condition for the region $a_i \le r \le a$ is applied as in the previous case, while the zero flux boundary condition for $0 \le r \le a_i$ is applied using:

$$C_2^{i=1,j} = \left(-C_S^{i=1,j}\right) = 1, \qquad D^{i=1,j} = 0$$

with notation as in the previous case. For the special cases of $a_i = 0$ the prescribed temperature case is used for the full lower surface, while for $a_i = a$ the zero flux boundary is uniformly applied.

v. For the cases considered in which insulation extensions protrude along the plane of the disk ($a_i > a$), zero flux boundaries are applied to the control volumes adjacent to the $\theta = \pi/2$ boundary. For those control volumes which contact the upper surface of this insulation, indexed by $(i, \frac{J}{2})$, the heat flux across the boundary is set to zero by allowing:

$$C_3^{i,\frac{J}{2}+\frac{1}{2}} = \left(-C_S^{i,\frac{J}{2}+\frac{1}{2}}\right) = 1, \qquad D^{i,\frac{J}{2}+\frac{1}{2}} = 0$$

where the superscript notation $i, \frac{J}{2} + \frac{1}{2}$ refers to the control surface coincident with the $\theta = \pi/2$ boundary. For those control volumes which contact the lower surface of the insulation (notation $(i, \frac{J}{2} + 1)$) a zero flux boundary is specified by:

$$C_4^{i,\frac{J}{2}+1-\frac{1}{2}} = \left(-C_S^{i,\frac{J}{2}+1-\frac{1}{2}}\right) = 1, \qquad D^{i,\frac{J}{2}+1-\frac{1}{2}} = 0$$

These homogeneous Neumann boundary conditions are applied for as many control volumes in the $i$ direction as are necessary to model the full radius of the insulation extension.

Thermal Constriction Resistance. Once the solution to the temperature field in the region surrounding the disk has been determined, the thermal constriction resistance can also be calculated. Since the numerical model is posed in oblate

spheroidal coordinates, a formulation of the dimensionless constriction resistance $R^*$ is required in these coordinates. The following expression for the dimensionless constriction resistance:

$$R^* = Rka = \frac{1}{2\pi \int_0^{m\pi} -\sin\theta \left.\frac{dT}{d\eta}\right|_{\eta=0} d\theta} \qquad (13)$$

where $m$ is some real positive value between 1/2 and 1 depending on the insulation radius $a_i$, is modified for the discrete numerical solution:

$$R^* = \frac{1}{2\pi \sum_{j=2}^{N} \left(\cos(\theta_{i,j-\frac{1}{2}}) - \cos(\theta_{i,j+\frac{1}{2}})\right) \frac{(T_0 - T_{i,j})}{(\Delta\eta)_{i-1,j}}} \qquad (14)$$

The summation is performed for the $N$ control volumes which bound the isothermal sections (both upper and lower) of the disk.

## Solution Accuracy and Convergence

In order to establish confidence in the numerical solution as presented, the three insulation cases for which exact solutions are available were examined. Introducing a non-dimensional insulation radius $\epsilon$, defined as insulation radius $a_i$ over disk radius $a$, the limiting cases, the isothermal disk in a full and half space corresponding to $\epsilon = 0$ and $\epsilon \to \infty$ show good agreement with the classical solutions(3): $R^* = 1/8$ and $1/4$, with percent difference between the numeric and exact values of 0.04% and 0.68% respectively. In order to further establish confidence in the numerical results, a closer study of the solution to the third case, that of the fully insulated back ($\epsilon = 1$) was undertaken. Using a grid of 100 by 100 control volumes, a numeric solution was performed which yielded a dimensionless constriction resistance within 1% of the exact solution $R^* = 1/2\pi$ (4). The convergence characteristics of this model are shown below on Figure 3.

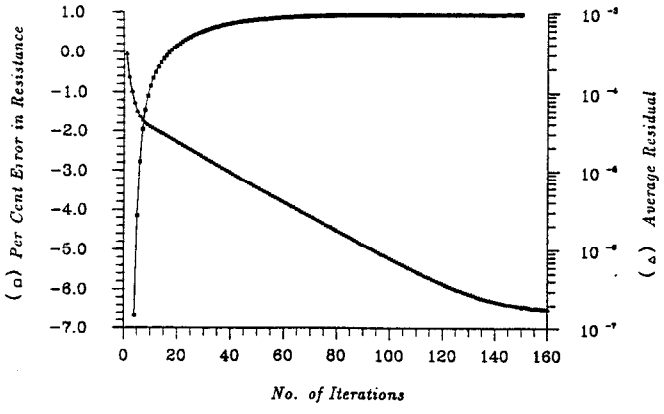


Fig. 3 Effect of Solution Iteration on Error in Resistance and Average Solution Residual

In order to quantify the convergence of the temperature field over the solution domain, an average solution residual is calculated for each iteration of the solver as presented on the graph. Defined as the average over the entire solution domain of the absolute values of the residual, it is determined using the following formulation for the residual of an arbitrary control volume $(i, j)$:

$$\delta_r = C_1 T_{i-1,j} + C_2 T_{i+1,j} + C_3 T_{i,j-1} + C_4 T_{i,j+1} + C_S T_{i,j} + D$$

In the ideal case, when convergence is achieved, the residual will reduce to zero for all control volumes in the solution domain. It can be seen from the plot that the average change in the field temperature as measured by the average solution residual decreases rapidly with increasing iteration. Complete convergence is assumed when the decrease of the average solution residual is halted by truncation errors caused by the single precision variables used.

Figure 3 also shows the percent error in resistance as plotted against the number of solution iterations. Using this curve it can be demonstrated that the dimensionless constriction resistance values converge quickly and successfully in the number of iterations performed.

In order to consider the dependence of solution accuracy on control volume size, the same case ($\epsilon = 1$) was considered while control volume size in both the $\eta$ and $\theta$ directions was varied. The results are given on Figure 4, where it can be seen that as discretization levels are increased in both coordinate directions, the percent error in resistance is decreased. Unlike

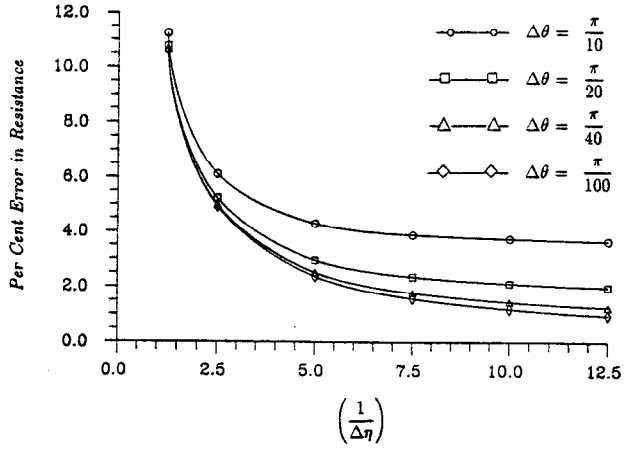


Fig. 4 Effect of Control Volume Size on Error in Resistance

the cases $\epsilon = 0$ and $\epsilon \to \infty$, which are reduced to a one-dimensional solution by the use of oblate spheroidal coordinates, this model shows a definite dependence on discretization in both coordinate directions. Increasing discretization to 150 control volumes in the $\eta$ direction and 250 control volumes in the $\theta$ direction yields a dimensionless resistance $R^* = 0.16007$, within 0.6% of the exact solution.

Based on these results it will be assumed that values of the thermal constriction resistance can be determined for any value of $\epsilon$ to within a fraction of a percent of their actual values if identical grid spacing and convergence criteria to the $\epsilon = 1$ case are used.

## Results

Having established a level of confidence in the accuracy of the numerical solution, the problem of varying insulation

levels may now be addressed. Using a 150 x 250 control volume model, the thermal constriction resistance was calculated numerically for a range of $\epsilon$ between 0 and 50. These results are shown on Figure 5 for a limited range of insulation values ($\epsilon < 4$). From this figure we observe that the increase in the dimensionless constriction resistance is gradual between $\epsilon = 0$ and $\epsilon \approx 0.7$; beyond this value the change becomes much more rapid. This large variation in $R^*$ continues to $\epsilon \approx 2$, where the change becomes more gradual again and the resistance approaches the half space value of 0.25.

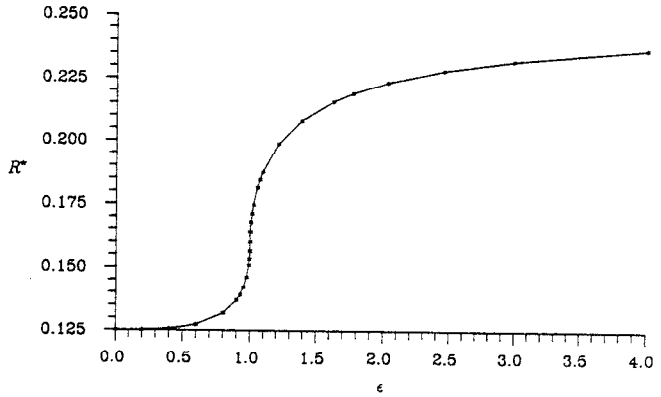


Fig. 5 Dimensionless Constriction Resistance versus Ratio of Insulation Radius to Disk Radius

Correlation Equations. Due to the complex nature of the dependence of the dimensionless constriction resistance $R^*$ on the insulation to disk radius ratio $\epsilon$ as shown in Figure 5, it was decided that two separate correlation equations should be formed, corresponding to the insulation cases $0 \leq \epsilon \leq 1$ and $1 \leq \epsilon < \infty$. The normalized solution data for the first interval $0 \leq \epsilon \leq 1$ is depicted on Figure 6. The independent variable $\epsilon$

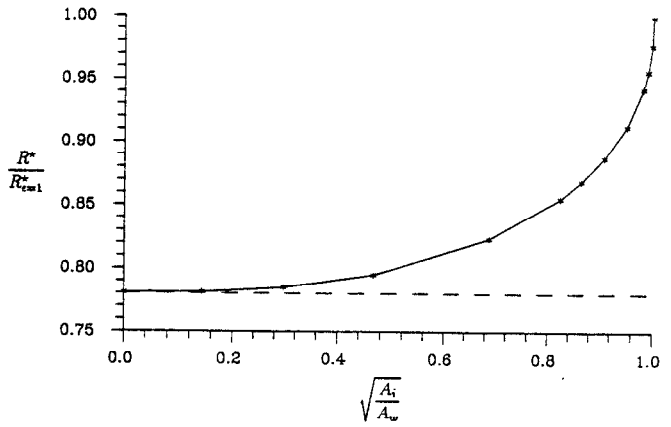


Fig. 6 Normalized Solution Data for Correlation Equation $0 \leq \epsilon \leq 1$

is transformed to the square root of the ratio of the insulated to wetted surface areas and the dependent variable $R^*$ is normalized by division by the exact solution for $\epsilon = 1$, $R^* = 1/2\pi$. A Gaussian error function was chosen for the correlation based on the shape and end characteristics of the resulting normalized curve. Using the general form:

$$\frac{\frac{R^*}{R^*_{\epsilon=1}} - 1}{\frac{\pi}{4} - 1} = erf\left(\zeta\sqrt{1 - \sqrt{A_i/A_w}}\right) \tag{15}$$

where $\pi/4$ and 1 are the lower and upper bounds of the normalized data, a value of $\zeta$ can be calculated to minimize correlation error for all data points. Calculating this optimized value and simplifying the equation gives:

$$2\pi R^* = 1 + \left(\frac{\pi - 4}{4}\right) erf\left(1.5804\sqrt{1 - \sqrt{\epsilon^2(2 - \epsilon^2)^{-1}}}\right) \tag{16}$$

which is valid in the region:

$$0 \leq \epsilon \leq 1$$

In order to normalize the solution data for the second case, it was recognized that the dimensionless constriction resistance asymptotically approaches the half-space solution as $\epsilon \to \infty$. The independent variable $\epsilon$ was therefore transformed using the inverse of the square root of the ratio of insulated to wetted surface areas. The dependent variable $R^*$ is treated in a similar fashion, using an inverse of the normalization from the previous case. The resulting data points are shown on Figure 7. Once again, the Gaussian error function was chosen

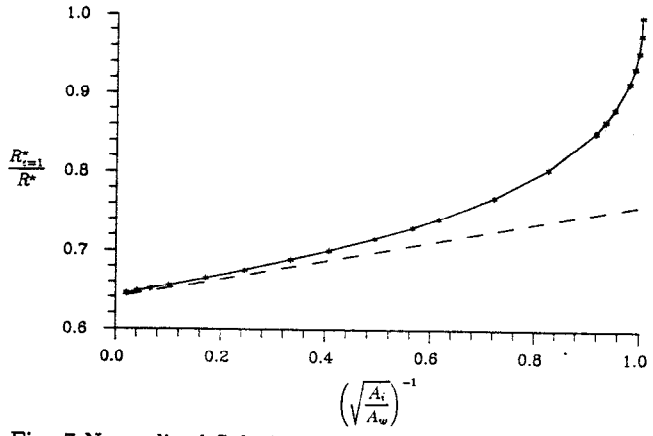


Fig. 7 Normalized Solution Data for Correlation Equation $1 \leq \epsilon < \infty$

for the correlation based on the nature of the curve but for this case it was recognized that the data approaches a linear function of the independent variable as $\epsilon \to \infty$. Using the general form:

$$\frac{\frac{R^*_{\epsilon=1}}{R^*} - 1}{\left(\frac{2}{\pi} + \xi\left(\sqrt{A_i/A_w}\right)^{-1}\right) - 1} = erf\left(\zeta\sqrt{1 - \left(\sqrt{A_i/A_w}\right)^{-1}}\right) \tag{17}$$

where 1 is the upper bound of the normalized data and the linear function $(2/\pi + \xi(A_i/A_w)^{-1/2})$ is the lower bound. As before, the values of $\zeta$ and $\xi$ are optimized and after simplification, the correlation can be expressed as:

$$\frac{1}{2\pi R^*} = 1 + \left[(0.14433\epsilon^{-1} + \frac{2}{\pi}) - 1\right] erf\left(2.32917\sqrt{1 - \epsilon^{-1}}\right) \tag{18}$$

which is valid in the region:

$$1 \leq \epsilon < \infty$$

These correlation equations will predict exact solutions at the three limiting cases, $\epsilon$ = 0,1, and $\rightarrow \infty$. For values in the range $0 < \epsilon < 0.6$ the correlation (Equation 16) and the numerical results differ by approximately one percent. For the remaining cases $0.6 < \epsilon < 1$, the difference between the correlation and numerical solution drops to within 0.3%. Equation 18 accurately predicts values within 0.8% of the numerical results over the whole range $1 < \epsilon < 50$.

Contour Plots of Isotherms and Heat Flux Vector Plots.
In an effort to describe the effects leading to the complex variation of dimensionless constriction resistance over the range of insulation values considered, contour plots of the temperature profiles and a vector plot of the heat flux distribution in the region immediately surrounding the disk were prepared, as shown in Figures 9-13 and Figure 14 respectively. All figures depict the region considered in non-dimensional polar coordinates within the limits:

$$0 \leq r/a \leq 2 \qquad -1 \leq z/a \leq 1$$

Temperature profiles for five cases, $\epsilon$ = 0.2, 0.8, 1.0, 1.2, and 2.0, and a heat flux vector plot for the case $\epsilon$ = 1.0 are presented in order to show the behavior of temperature and heat

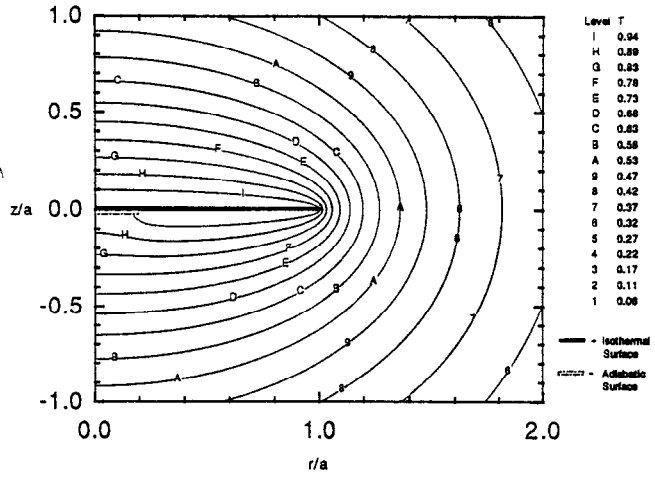


Fig. 9 Temperature Profile from Numerical Solution $\epsilon$ = 0.2

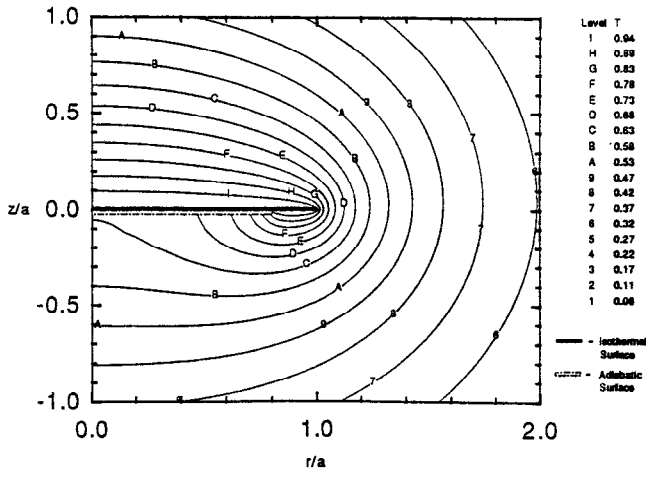


Fig. 10 Temperature Profile from Numerical Solution $\epsilon$ = 0.8

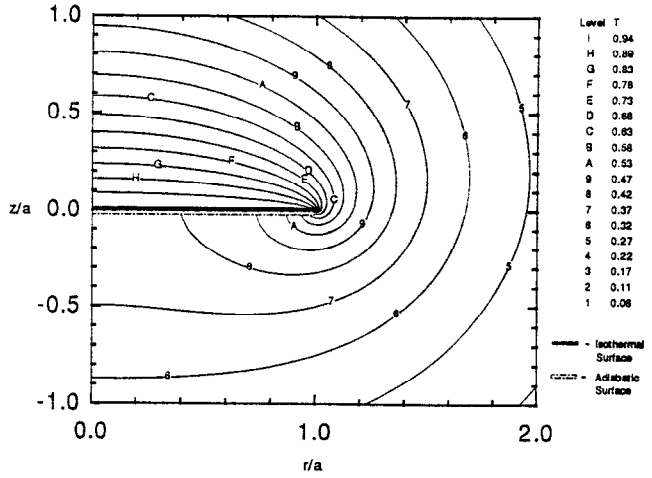


Fig. 11 Temperature Profile from Numerical Solution $\epsilon$ = 1.0

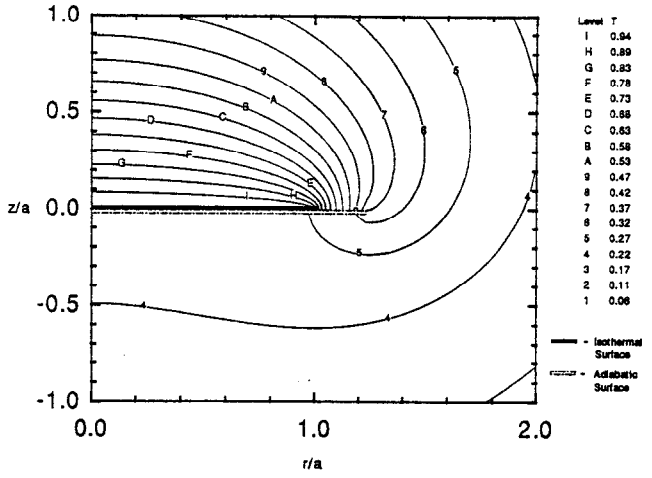


Fig. 12 Temperature Profile from Numerical Solution $\epsilon$ = 1.2

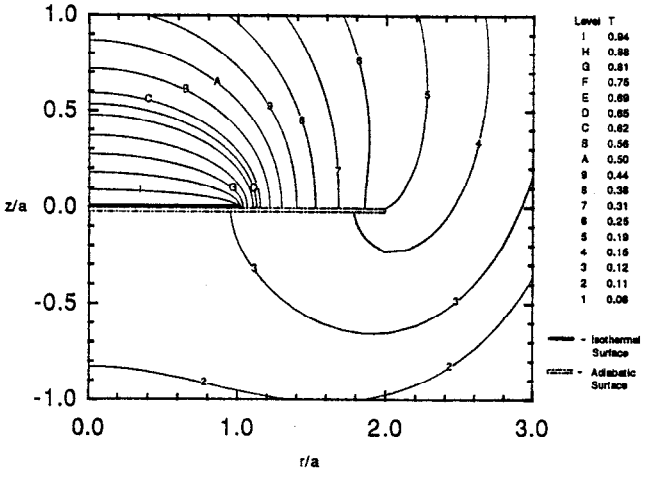


Fig. 13 Temperature Profile from Numerical Solution $\epsilon$ = 2.0

flux in the region surrounding the disk for values near the fully insulated back limit as well as for those values approaching the full and half space solutions.

The heat flux vector plot presented in Figure 14 is a graphical representation of the following expressions, as formulated in oblate spheroidal coordinates:

$$\vec{q}_\eta = \frac{-k\vec{a}_\eta}{a(\cosh^2\eta - \sin^2\theta)^{1/2}}\frac{dT}{d\eta}, \quad \vec{q}_\theta = \frac{-k\vec{a}_\theta}{a(\cosh^2\eta - \sin^2\theta)^{1/2}}\frac{dT}{d\theta}$$

where $\vec{a}_\eta$ and $\vec{a}_\theta$ are unit vectors in the $\eta$ and $\theta$ directions respectively. These equations are solved for interior control volumes using the temperature values at surrounding nodes; no vectors are included to represent boundary fluxes. Each vector displayed in Figure 14 starts at a nodal point and each has length corresponding to its magnitude. The exception to this convention occurs in the region near the outer edge of the disk, where vector length has been limited within the boxed sections. Accurate representation of vector magnitudes for these regions is given in the zoomed views.

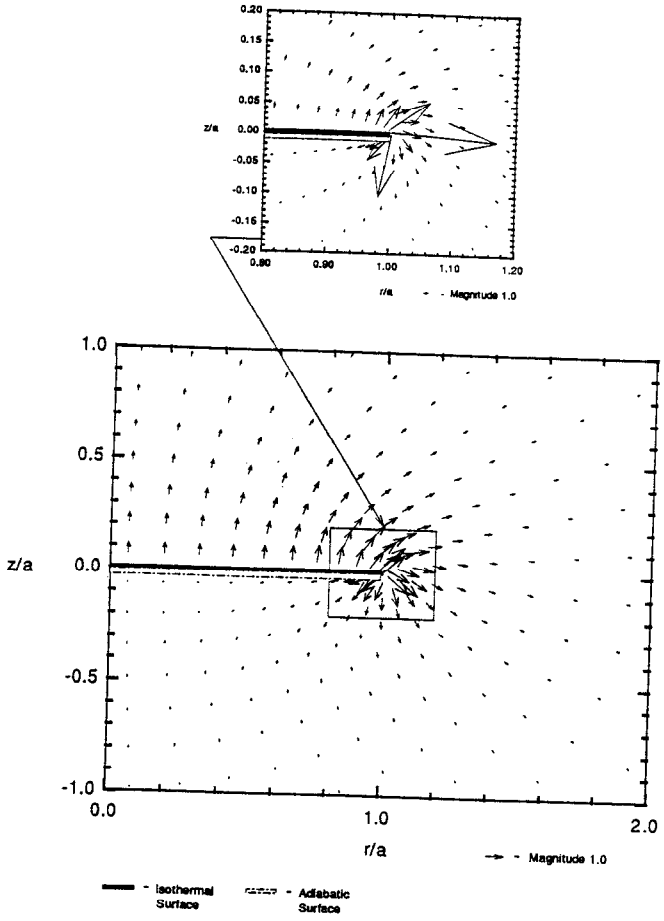


Fig. 14 Heat Flux Vector Plot from Numerical Solution $\epsilon = 1.0$

From both the contour and vector plots it can be shown that relatively small changes in the dimensionless insulation radius near $\epsilon = 1$ have large effects in both the temperature and flux distributions in the region directly below the disk. The isotherms of the insulation case $\epsilon = 0.8$ resemble those of $\epsilon = 0.2$ while the plots for $\epsilon = 1.2$ and $\epsilon = 2.0$ show both similarities to each other and differences from the partially insulated cases. It becomes clear that the extremely large fluxes that occur at the outer edge of the disk as shown in Figure 14 dominate the total heat flow from the body, and small changes in the boundary conditions in this region will have a dramatic effect on the surrounding temperature field.

## SUMMARY AND CONCLUSIONS

A numerical model for analysis of heat conduction from an isothermal circular disk in a full space with mixed boundary conditions on its lower surface has been developed using the method of finite volumes in an oblate spheroidal coordinate system. The accuracy of the numeric results is good, as verified by comparison to the exact solutions at the full space ($\epsilon = 0$), half space ($\epsilon \to \infty$), and fully insulated back ($\epsilon = 1$) limits, where differences of 0.04%, 0.6%, and 0.68% are calculated, respectively. Based on these results and using the same spatial discretization and convergence criteria as these models, it is assumed that the solutions to other cases $0 < \epsilon < \infty$ will have comparable accuracy.

The analysis also revealed that for cases where insulation extensions are not infinite, good results may still be obtained using the exact half space solution to approximate the thermal constriction resistance of the system. For $\epsilon \geq 6$, this assumption predicts the numerical solution to the dimensionless constriction resistance $R^*$ to within 4% of its exact value, while for $\epsilon \geq 10$ , the error is reduced to less than 2.5%.

The results of the numerical model are used in order to formulate two correlation equations for the prediction of the dimensionless constriction resistance $R^*$ from the insulation radius ratio $\epsilon$. These equations yield exact values at their limits and, for most other cases, accurately predict the numeric solutions to within 1%.

## ACKNOWLEDGEMENTS

The authors acknowledge the financial support of the Natural Sciences and Engineering Research Council of Canada under operating grant A7455 for Dr. Yovanovich.

## REFERENCES

1. Schneider, G.E., "Discrete Methods in Heat Conduction: a Review," Advances in Transport Processes, Vol. 3, Wiley Eastern, New Delhi, 1984, pp. 122-130. Editors, Mujamdar, A.S., and Mashelkar, R.A.

2. Strong, A., Schneider, G., and Yovanovich, M.M., "Thermal Constriction Resistance of a Disc With Arbitrary Heat Flux - Finite Difference Solution in Oblate Spheroidal Coordinates," *AIAA* Progress in Astronautics and Aeronautics, Heat Transfer with Thermal Control Applications, MIT Press, Vol. 39, pp. 65-78, 1975. Editor, Dr. M.M. Yovanovich, University of Waterloo.

3. Carslaw, H.S., and Jaeger, J.C., Conduction of Heat in Solids, 2nd ed., Clarendon Press, London, 1959, pp. 215-217.

4. Lemczyk, T.F., through personal communication.